Contents lists available at ScienceDirect

Arabian Journal of Chemistry

journal homepage: www.ksu.edu.sa

Original article

Interaction and binding mechanism of anticancer echinacoside phenylethanoid glycoside against hepatocellular carcinoma with subdomains of human serum albumin

Liguo Xu *, Wenhao Huang *, Yachao Lin *, Zhendong Li

Interventional Medicine Department, The Second Affiliated Hospital of Zhengzhou University, Zhengzhou 450014, China

ARTICLE INFO

Keywords:
Echinacoside
Liver cancer
Interaction
Albumin
Anticancer

ABSTRACT

A phenylethanoid glycoside known as echinacoside has demonstrated promising anticancer properties against numerous cancer cell types. However, its pharmacokinetics or anticancer mechanism has remained unclear. Herein, the interaction of the echinacoside with human serum albumin (HSA) was explored by intrinsic/extrinsic fluorescence spectroscopy, circular dichroism (CD) spectroscopy as well as molecular docking simulation. Also, the anticancer effects and possible mechanism of action of the echinacoside against hepatocellular carcinoma (HCC) cells, MHCC-97-H with high tumorgenicity and metastasis, were assessed by cell viability, flow cytometry, qRT-PCR, and western blot assays. The results showed a static quenching mechanism in the formation of echinacoside-HSA complex, one binding site on HSA for echinacoside, contribution of hydrophobic interactions (PHE157, GLU188 and PRO447), and slight conformational changes of HSA in the complex form. Cellular assays disclosed that treatment with echinacoside concentration-dependently mitigated the proliferation of MHCC97-H cells *in vitro* with an IC_{50} concentration of around 30 μM. Also, echinacoside triggered apoptosis through the regulation of caspase-3 at mRNA and protein levels. Moreover, echinacoside reduced the expression of astrocyte elevated gene-1 (AEG-1) and N-cadherin, while enhancing the expression of E-cadherin, as the main hallmarks of epithelial–mesenchymal transition (EMT) in tumorigenicity and metastasis. Therefore, these data indicated that echinacoside with a promising binding affinity with HSA in a mimicking physiological condition may inhibit the proliferation and metastatic activity of MHCC97-H cells mediated by manipulation of the AEG-1/EMT pathway.

1. Introduction

Echinacoside as a phenylethanoid glycoside isolated from *Echinacea angustifolia* (Liu et al., 2018) has a molecular formula of $C_{35}H_{46}O_{20}$ with a molecular weight of 786.7 g/mol. Echinacoside has been widely examined for the regulation of Parkinson's (Liang et al., 2019), Alzheimer's (Dai et al., 2020), cognitive impairment (Qiu and Liu, 2022), Hirschsprung's (He et al., 2023), bone regeneration (Li et al., 2012), and hypoxic pulmonary hypertension (Gai et al., 2020). Echinacoside can trigger anticancer activities against a broad range of cancer cells including breast (Tang et al., 2020), colorectal (Dong et al., 2015a), lung (Shi et al., 2022, Cao et al., 2023), liver (Li et al., 2021), ovarian (Liu et al., 2022), and pancreatic adenocarcinoma (Wang et al., 2022) through regulating the Wnt/β-catenin signaling pathway, induction of oxidative DNA damages, mitochondria-mediated pyroptosis, miR-503-3p/TGF-β1/Smad axis, PI3K/AKT, and mitogen-activated protein kinase pathways, respectively.

Among the most common malignant tumors, hepatocellular carcinoma (HCC) is often diagnosed at an advanced stage and has a high incidence and mortality rate. Invasiveness and metastasis are the main causes of poor prognosis among HCC patients and high mortality rates (Zheng et al., 2014a, Li et al., 2014). Preventing invasion and metastasis of HCC could be recruited as a potential strategy for reducing mortality and manipulating its progression. Metastasis and invasion of tumors are known as multi-step processes resulting in the patient's death. Metastasis of a tumor includes four main steps including separation, circulation, adhesion, and invasion to the target tissues (Zheng, Li et al., 2014). Any compound blocking these processes can be nominated as a useful candidate in inhibiting cancer metastasis. Several studies have shown that echinacoside could exert anti-tumor activity in liver cancer cells mediated by iR-503-3p/TGF-β1/Smad axis (Li et al., 2021), TREM2 expression and PI3K/AKT signaling (Ye et al., 2019), targeting UBR5

* Corresponding authors at: NO.2, Jingba Road, Zhengzhou 450014, China.
E-mail addresses: xuliguo8@163.com (L. Xu), Yachaolinn@outlook.com (Y. Lin).

https://doi.org/10.1016/j.arabjc.2024.105869
Received 13 May 2024; Accepted 9 June 2024
Available online 15 June 2024

(Wang et al., 2022), and inhibiting the nucleotide pool sanitizing enzyme MTH1 (Dong, Wang et al., 2022). However, no study has been published on the suppression of hepatocarcinoma MHCC97-H cells showing highly metastatic potential mediated by inhibition of epithelial–mesenchymal transition (EMT) and astrocyte elevated gene-1 (AEG-1) pathway. Morphology as well as invasion of HCC alter following blocking AEG-1 expression (Zheng, Li et al., 2014). Indeed, AEG-1 mRNA upregulation and EMT appearance occur in HCC tissues, which are known as potential markers in cancer development and metastasis (Zheng, Li et al., 2014).

On the other hand, the interaction of therapeutic compounds/drugs with blood protein can provide useful information about their pharmacokinetics properties *in vitro*. Plasma protein binding can be determined as a general approach for modulating the pharmacokinetics of proteins as well as drugs (Dennis et al., 2002, Zhang et al., 2019, Pilati and Howard, 2020). Human serum albumin (HSA) binding affinities can be used as a potential procedure to regulate the pharmacodynamics and pharmacokinetics of drug candidates (Fan et al., 2022). This led different researchers to analyze the interaction of different small molecules/drugs/compounds with HSA (Yamasaki et al., 2013, Chuang et al. 2013, Xue et al., 2021, Yu et al., 2022).

Therefore, in this study, first, we evaluated the interaction of the echinacoside with HSA by different experimental and theoretical assays to determine the binding affinity and unwanted protein structural changes. Furthermore, the anticancer and antimetastatic effects of the echinacoside in MHCC97-H as a model of HCC were assessed.

2. Materials and methods

2.1. Materials

Free albumin from human serum (HSA, product number: A1653, ≥96 % with agarose gel electrophoresis), echinacoside (product number: 07668, ≥98 % HPLC), 3-(4,5-dimethylthiazol-2-yl)-2,5-diphenyl tetrazolium bromide (MTT, CAS No. 298–93-1), and dimethyl sulfoxide (DMSO, ≥ 99.9 %, CAS No. 67–68-5) were obtained from Sigma-Aldrich Co. (St Louis, MO, USA). All other materials were of analytical reagent grade and used without further purification/analysis.

2.2. Preparation of working solutions

HSA stock solution was prepared in sodium phosphate buffer (20 mM, pH 7.4) and the concentration was determined using a well-known spectrophotometric method ($\varepsilon_m = 36{,}500\ M^{-1}\ cm^{-1}$ at 280 nm) (Tayyab et al., 2019). Echinacoside stock solution was obtained in dimethylsulfoxide (DMSO) and working solutions were prepared by diluting the stock samples with sodium phosphate buffer (20 mM, pH 7.4) or cell culture medium. All aqueous solutions were obtained with freshly double-distilled water.

2.3. Fluorescence quenching study

HSA fluorescence spectra were recorded on a PerkinElmer LS55 luminescence spectrometer (PerkinElmer Inc., Waltham, MA, USA). The exaction wavelength was set at 295 nm, while spectral bandwidths were fixed at 10 and 5 nm for excitation and emission, respectively. The fluorescence spectra of HSA were read in the wavelength range of 300–440 nm. The HSA solution was added by increasing concentrations of the echinacoside (2–60 μM). All fluorescence experimental parameters were kept unchanged during each data set. Fluorescence spectra were recorded in quartz cuvettes with a path length of 1 cm. Titration experiments were carried out manually employing a micropipette. Also, for each spectrum, the fluorescence emission of protein either alone or with echinacoside was read with HSA at the final concentration of 2.0 μM.

The fluorescence emission spectra were corrected using the following Eq. (1) (Zhang et al., 2019):

$$Fo = Fc \times 10(A1 + A2)/2 \quad (1)$$

Where F_o and F_c are the observed and corrected fluorescence intensity, respectively. Also, A_1 and A_2 are the absorption of solutions at the excitation and emission wavelengths, respectively (Zhang et al., 2019).

2.4. Synchronous fluorescence study

Synchronous fluorescence spectra of HSA in the presence or absence of the echinacoside were read by scanning the excitation and emission monochromator simultaneously with fixing $\Delta\lambda = 15$ nm and $\Delta\lambda = 60$ nm as reported previously (Yekta et al., 2017). The excitation and emission slit widths were fixed at 10 nm and 5 nm, respectively.

2.5. Circular dichroism study

To study the effects of binding echinacoside on the secondary structure of HSA, the far-UV circular dichroism (CD) spectra of HSA (190–260 nm) were used. HSA and echinacoside samples were diluted in sodium phosphate buffer (20 mM, pH 7.4). The concentration of HSA was 5 μM and the protein solution was titrated with increasing concentrations of the echinacoside (2–60 μM). The CD data were collected on a J-810 spectropolarimeter (Jasco, Tokyo, Japan), using a 1 mm cell at room temperature under constant nitrogen flush. The scan rate, bandwidth and response time scan rate were fixed at 200 nm/min, 1 s and 1 nm, respectively (Yekta et al., 2017). The alterations in the percentage of secondary structure amount of HSA were calculated using CDNN software.

2.6. Molecular docking study

To analyze the interaction between HSA with echinacoside, we have used a molecular docking study. We used AutoDock for molecular docking simulation and AutoDock tools to design the files for this study. The three-dimensional (3D) HSA structure (chains A and B) was obtained from the Protein Data Bank, PDB ID: 1AO6. Seven water molecules were removed from the protein structure and the 3D structure of the echinacoside compound was downloaded from the PubChem compound database (CID 5281771). Polar hydrogen atoms and charges were added to the echinacoside and HSA structures. The cavity volume was set to 20892 A^3 and the grid center coordinates were 24, 15 and 22 for X, Y and Z coordinates, respectively. All other parameters were fixed as default values. During molecular docking simulation, the HSA molecule was kept rigid and the echinacoside was flexible. The total number of runs was set at 5. The protein–ligand complexes with pocket RMSD ≤ 4 Å in the ligand binding site were assessed for the molecular docking simulation analysis.

2.7. Cell culture

The human HCC cell line, MHCC97-H, was purchased from the American Type Culture Collection (ATCC, Manassas, VA, USA) and cultured in high-glucose DMEM (GIBCO, USA) containing 100 U/mL penicillin and 10 μg/ml streptomycin with 10 % heat-inactivated fetal bovine serum (FBS, PAN-Biotech, Aidenbach, Germany).

2.8. MTT assay

The MTT assay was done to quantify the effect of the echinacoside on cell viability. Briefly, MHCC97-H (1×10^4cells/well) cells plated on a 96-well plate at 37 °C were exposed to different concentrations of the echinacoside (0–60 μM). After incubation for 24 h, the medium was removed and cell viability was assessed by the MTT assay as described previously (Zheng, Li et al., 2014).

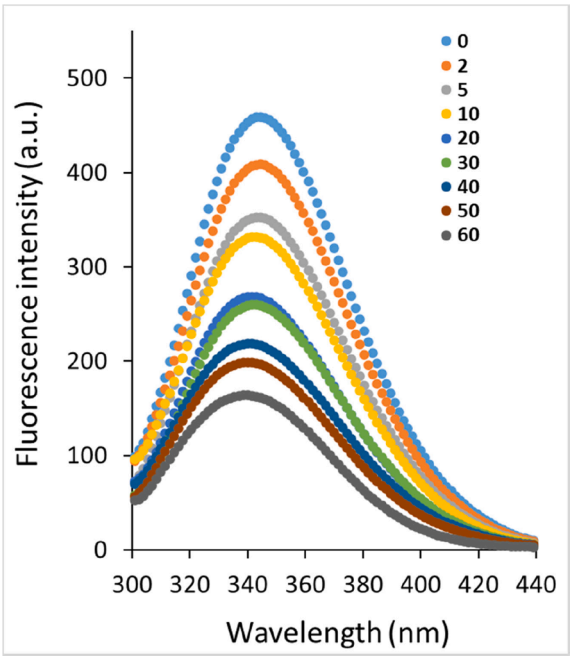

Fig. 1. Fluorescence quenching study of HSA following addition of increasing concentrations of the echinacoside at 298 k.

2.9. Flow cytometry assay

To detect apoptosis, the cells were incubated with PI/fluorescein isothiocyanate (FITC)-conjugated annexin V based on the manufacturer's instructions by Annexin V-FITC Apoptosis Detection Kit I (Becton Dickinson, San Jose, CA, USA). Briefly, after adding the appropriate concentration of the echinacoside (IC_{50}) and incubating for 24 h, the cells were harvested, washed with PBS, resuspended in 50 µl of 1 × binding buffer containing 5 µl of annexin V-FITC and 10 µl of PI, incubated in the dark for 15 min, added by 450 µl of 1 × binding buffer, kept on ice, and subjected to flow cytometry analysis (Becton Dickinson, San Jose, CA, USA).

2.10. Quantitative reverse transcription polymerase chain reaction (qRT-PCR)

MHCC97-H cells seeded in a six-well plate were treated with IC_{50} concentration of echinacoside for 24 h. Total RNA was then extracted using the Trizol reagent (Invitrogen) following the manufacturer's protocols, followed by RNA quantification assay using Nanodrop® Spectrophotometer (Thermo Fisher). cDNA Reverse Transcription kit was used for the synthesis of cDNA following the manufacturer's protocol (Applied Biosystems). Primers for caspase-3 and housekeeping gene β-actin and the annealing temperature of the genes were designed/used as previously reported (Gao et al., 2014). qRT-PCR analysis was then performed using an Express SYBR qPCR Supermix (Invitrogen) following the manufacturer's protocol on an Applied Biosystems Real-Time PCR System. Relative expression of mRNA was expressed by the comparative CT method.

2.11. Western blot analysis

The cells in a six-well plate incubated with echinacoside (IC_{50}) for 24 h, were exposed to lysis buffer (Cell Signaling Technology, Danvers, MA, USA) based on the manufacturer's protocols containing some inhibitors. The protein concentrations of the samples were determined on a Bio-Rad DC protein kit (Bio-Rad Laboratories, USA). The cell lysates in equal amounts were then subjected to electrophoresis by SDS-PAGE, followed by western blotting analysis using antibodies against AEG-1 (13860–1-AP, Zhongshan Goldenbridge Biotechnology Co., Ltd. Beijing, China), E-cadherin (BS1098, Bioworld Technology, Inc. Louis Park, MN, USA), N-cadherin (BS2224, Bioworld Technology, Inc. Louis Park, MN, USA), caspase-3 P17 (Santa Cruz Biotechnology, Santa Cruz, CA, USA), and β-actin (AP0060, Bioworld Technology, Inc. Louis Park, MN, USA) overnight at 4 °C. The samples were then incubated for 1 h with HRP-conjugated secondary antibodies at room temperature (Santa Cruz, Heidelberg, Germany), and the antibody-reactive bands were then detected on an ECL system (Amersham Biosciences, Piscataway, NJ, USA).

2.12. Statistical analysis

The data are expressed as the means ± SD of at least three assays and analyzed via one-way ANOVA using the SPSS software. Differences with $P < 0.05$ were considered statistically significant. The baseline signals (buffer and echinacoside) were subtracted from all analyses.

3. Results and discussion

3.1. Fluorescence quenching study

The fluorescence experiments were carried out to examine the interaction mechanism of the echinacoside to HSA. Fluorescence quenching is known as a potential and straightforward strategy to study the interaction between particles and macromolecules, especially plasma proteins. This method could provide us with valuable details regarding the quenching mechanism, binding affinities, and thermodynamic parameters (Zeinabad et al., 2016). The fluorescence quenching is named based on the decline of fluorescence intensity, which could derive from different molecular interactions (Yammine et al., 2019). The intrinsic fluorescence of HSA stems from aromatic amino acid residues, mainly tryptophan (Trp) and tyrosine (Tyr) residues. Indeed, in the fluorescence analysis, when the excitation wavelength fixes at 295 nm, the emission fluorescence intensity from HSA mostly corresponds to its main intrinsic fluorescent amino acid residue, Trp (Yammine et al., 2019). Based on these facts, we set the excitation wavelength at 295 nm to determine the type of quenching mechanisms and other interaction parameters responsible for the formation of echinacoside-HSA complex. The maximum emission intensity for the HSA was determined to be around 344 nm at 298 K when protein samples were excited at 295 nm (Fig. 1). As displayed in Fig. 1, the emission of HSA was continuously quenched following the addition of increasing concentrations of the echinacoside at 298 K in 20 mM sodium phosphate buffer (pH 7.4).

Also, a blue shift (344 nm to 340 nm) was detected following addition of increasing concentrations of the echinacoside. These data disclosed that the microenvironment of the aromatic residues in HSA may be altered following interaction with echinacoside, which needs further studies. Quenching mechanisms are mostly classified as static, dynamic, or mixed. When temperatures are higher and diffusion is faster, collisions are more likely to occur. As a result, the dynamic quenching constant may rise with increasing temperature. With increasing temperature, however, the stability of the complexes declines, resulting in lower static quenching constants (Laws and Contino, 1992, Kumar et al., 2006). To determine the type of fluorescence quenching mechanism, the quenching data derived from the fluorescence study were assessed according to the well-known Stern-Volmer Eq. (2) (Geethanjali et al., 2015):

$$F\text{HSA}/F\text{HSA} - \text{echinacoside} = KSV\,[\text{echinacoside}] + 1 = kq\tau 0 + 1 \quad (2)$$

where F_{HSA} and $F_{HSA\text{-echinacoside}}$ define the fluorescence intensities of the HSA and HSA-echinacoside, respectively. K_{SV} and [echinacoside] define the Stern-Volmer quenching constant and concentration of the echinacoside, k_q displays the quenching rate constant, and τ_0 defines the

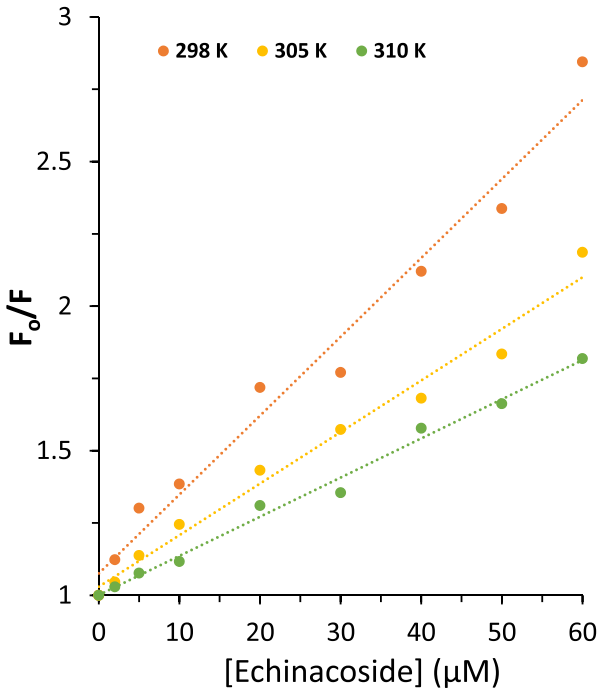

Fig. 2. Stern-Volmer plots of HSA following addition of increasing concentrations of the echinacoside at three temperatures.

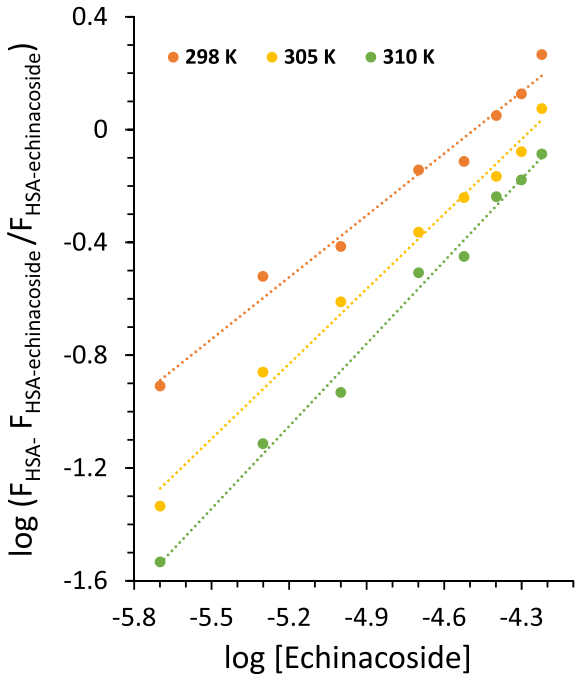

Fig. 3. Modified Stern-Volmer plots of HSA following addition of increasing concentrations of the echinacoside at three temperatures.

Table 1
Quenching constants for the interaction of the echinacoside with HSA at 298, 305 and 310 K.

T(K)	K_{SV} ($\times 10^4$ L mol^{-1})	k_q ($\times 10^{12}$ L mol^{-1} s^{-1})	R^2
298	2.73	2.73	0.9765
305	1.78	1.78	0.981
310	1.35	1.35	0.9914

R^2 is the correlation coefficient, K_{SV} is Stern-Volmer quenching constant and k_q is the quenching rate constant.

Table 2
Binding parameters for the interaction of the echinacoside with HSA at 298, 305 and 310 K.

T(K)	$logK_b$	n	R^2
298	3.27	0.73	0.9801
305	3.77	0.88	0.9898
310	4.01	0.97	0.992

R^2 is the correlation coefficient, K_b is the binding constant, and n is the number of binding sites.

fluorescence lifetime, which is $\simeq 10^{-8}$ s for HSA (Holovko et al., 2023).

Fig. 2 depicts the Stern-Volmer plots for the interaction of HSA following interaction with increasing concentrations of the echinacoside at 298, 305, and 310 K. Eq. (2) was employed to compute K_{SV} values based on a linear regression plot of F_0/F versus [echinacoside].

Then, the quenching parameters were determined at three different temperatures and the resultant K_{SV} and K_q values are listed in Table 1.

As observed in Table 1, the K_{SV} values for the interaction of the echinacoside with HSA were 2.73×10^4 L mol^{-1}, 1.78×10^4 L mol^{-1} and 1.35×10^4 L mol^{-1} at 298, 305, and 310 K, respectively.

As a consequence, this case appears to have a dominant static quenching mechanism due to the reduction of K_{SV} values at high temperatures. In addition, the maximum dynamic quenching constant, k_q, for protein–ligand interaction is $\simeq 2.0 \times 10^{10}$ M^{-1} s^{-1}. The k_q values computed at 298, 305, and 310 K for the interaction of the echinacoside with HSA were much greater than 2.0×10^{10} M^{-1} s^{-1} (Paliwal et al., 2023), suggesting that static quenching predominated in this experiments (Flores-Rivera et al., 2023).

3.2. Determination of binding parameters and binding forces

For the static quenching binding between a protein and ligand, the n and K_b refer to the number of binding sites and binding constant, *respectively,* can be determined according to the following Eq. (3) (Yekta et al., 2017):

$$\log(FHSA - FHSA - \text{echinacoside}/FHSA - \text{echinacoside}) = \log Kb + n\log[\text{echinacoside}] \quad (3)$$

where F_{HSA} and $F_{HSA\text{-echinacoside}}$ define the fluorescence intensities of the HSA and HSA-echinacoside, respectively and [echinacoside] is the total concentration of ligand. Then, the K_a and n values were estimated from plotting log (F_{HSA}- $F_{HSA\text{-echinacoside}}$ /$F_{HSA\text{-echinacoside}}$) versus log [echinacoside] (Fig. 3). The values of Y-intercept and slope were associated with logK_b and n values, respectively (Fig. 3). Table 2 summarizes the computed K_a and n values.

The n value was determined to be $\simeq 1$ at 310 K (Table 2), suggesting that one molecule of the echinacoside binds with one molecule of HSA (Yekta et al., 2017, Li, Yan et al. 2023). HSA shows one binding site for echinacoside. Also, if the first binding molecule reduces the bio-affinity of the second site, negative cooperativity occurs upon the interaction of ligand and protein reflected by $n < 1$. It implies that at 298 K, such binding may be possible due to the $n = 0.73$ (Table 2), which indicates negative cooperativity in the binding process of the echinacoside to HSA at low temperature (Tyukodi et al., 2023, Wang et al., 2023).

At 310 K, the binding constant, K_b, was calculated to be $\simeq 10^4$ L/mol (Table 2), suggesting that there is a moderate interaction between echinacoside and HSA (Kaur et al., 2023, Menezes et al., 2023).

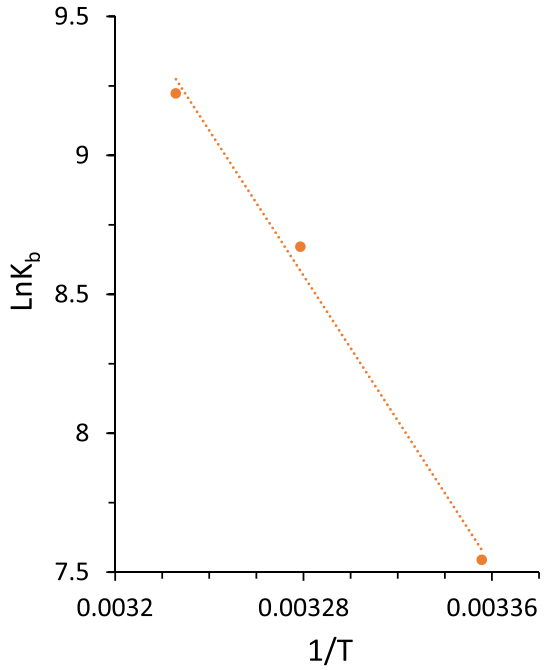

Fig. 4. van't Hoff plot of HSA following addition of increasing concentrations of the echinacoside.

Table 3
Thermodynamic parameters for the interaction of the echinacoside with HSA.

T(K)	ΔH° (KJ mol^{-1})	ΔS° (Jmol^{-1} K^{-1})	ΔG° (KJ mol^{-1})
298			−18.75
305	108.30	426.37	−21.73
310			−23.86

3.3. Thermodynamic parameters

Increasing the value of K_b induced by raising temperature reveals an endothermic interaction between the HSA and echinacoside (Table 2) (Yekta et al., 2017). There are several types of binding forces between ligands and biomacromolecules, including hydrogen bonds, hydrophobic bonds, electrostatic interactions, and van der Waals interactions (Yekta et al., 2017). Typically, binding modes are determined using thermodynamic parameters [standard enthalpy change (ΔH°), standard entropy change (ΔS°), and standard free energy change (ΔG°)] (Zeinabad et al., 2016). If ΔH° and ΔS° are both negative, hydrogen bonding and van der Waals interactions may play a key role in the interaction process, while if both values are positive, hydrophobic interactions are dominant. If ΔH° values are negative and ΔS° values are positive, these may imply that electrostatic interactions are the main contributing forces in the particle-biomacromolecule reaction (Zeinabad et al., 2016). The thermodynamic parameters were then calculated for the interaction between the echinacoside and HSA using van't Hoff and Gibbs-Helmholtz Eqs. (4, 5):

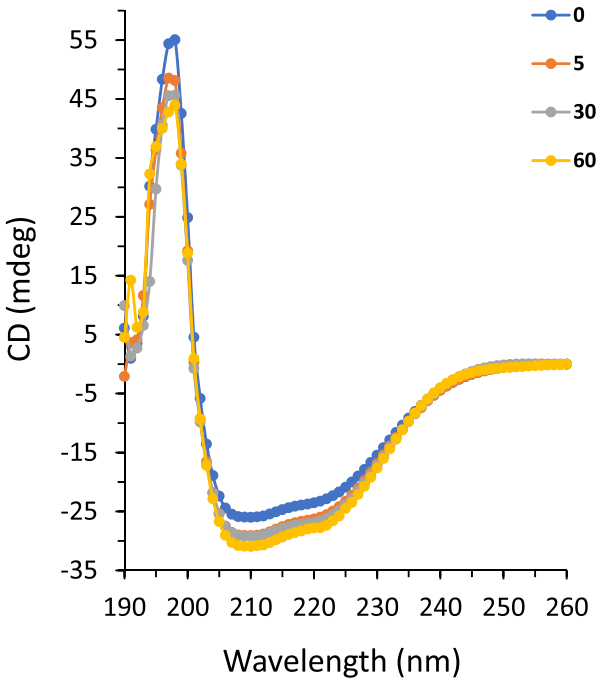

Fig. 6. CD spectra of HSA following interaction with increasing concentrations of the echinacoside.

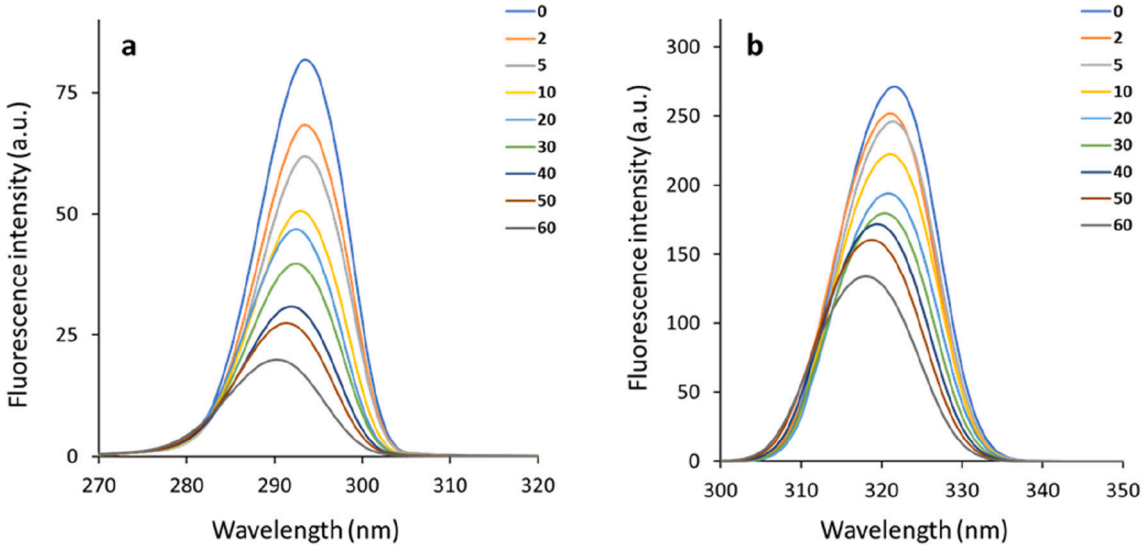

Fig. 5. Synchronous fluorescence spectra of HSA's Tyr (Δλ = 15 nm, a) and Trp (Δλ = 60 nm, b) residues following interaction with increasing concentrations of the echinacoside.

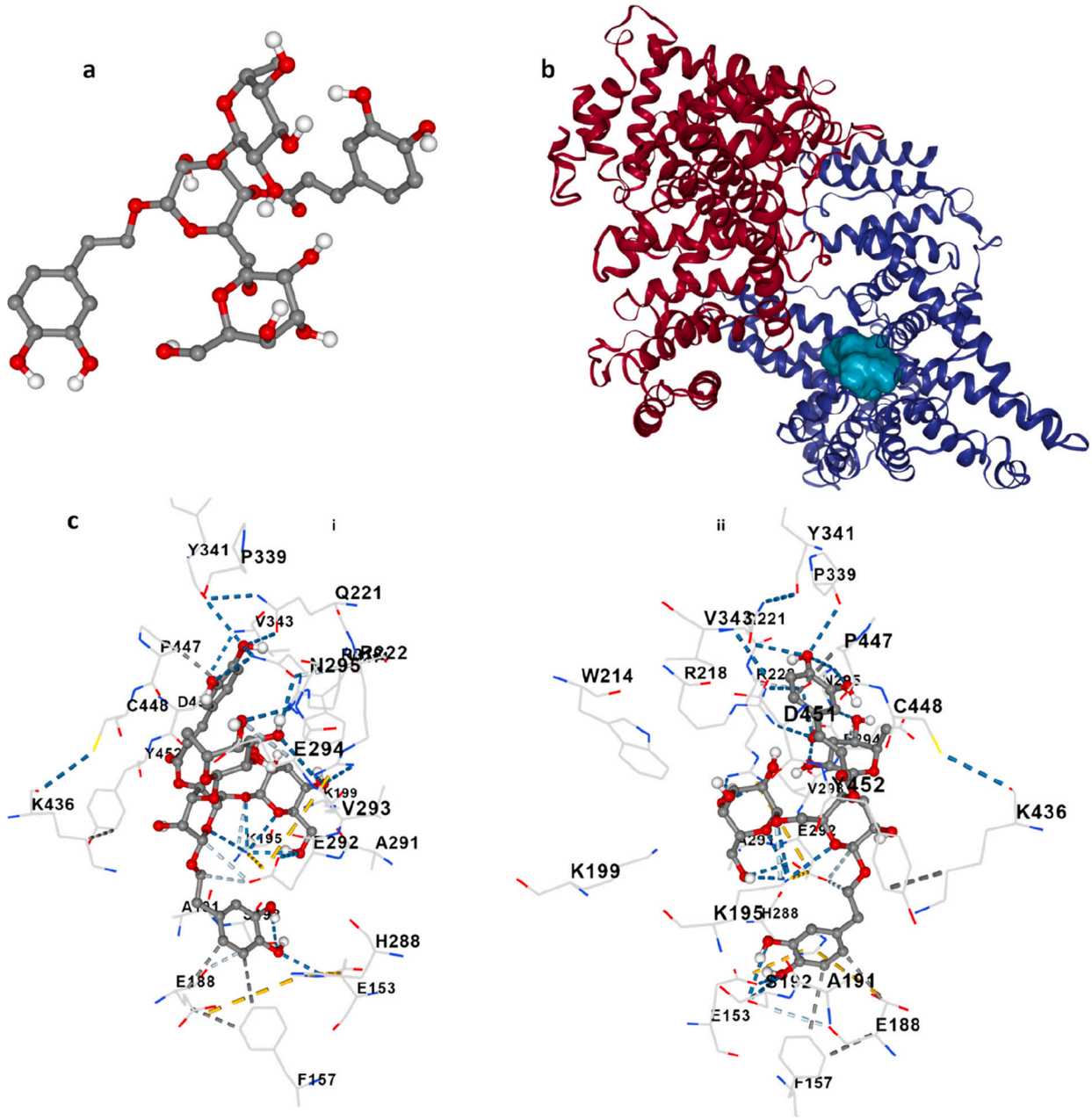

Fig. 7. Molecular docking study of HSA following interaction with echinacoside. Echinacoside structure (a), HSA- echinacoside complex (b), and amino acid residues in the binding pocket at two sides (c, i, ii).

$$\ln Kb = -\Delta H^{\circ}/RT + \Delta S^{\circ}/R \quad (4)$$

$$\Delta G^{\circ} = \Delta H^{\circ} - T\Delta S^{\circ} \quad (5)$$

where R is the universal gas constant, and T is the absolute temperature. The thermodynamic parameters of the echinacoside-HSA complex were determined based on Fig. 4 and the data were listed in Table 3.

The negative values of ΔG° at all temperatures designate that the binding of the echinacoside to HSA is driven by a spontaneous reaction. The calculated positive values of ΔH° (108.30 KJ mol^{-1}) and ΔS° (426.37 J mol^{-1} K^{-1}) indicated that the hydrophobic interactions may play a key role in the formation of the echinacoside-HSA complex (Zeinabad et al., 2016).

3.4. Synchronous fluorescence studies

We can obtain important details about the molecular environment surrounding the HSA chromophore groups by analyzing the synchronous fluorescence spectra. The corresponding red/blue shift in the maximum emission (λ_{max}) position is attributed to converting the polarity changes surrounding chromophores. A red or blue shift of λ_{max} indicated that the amino acid residues are more or less exposed to the solvent, respectively (Yekta et al., 2017, Hu et al., 2023).

The conformational changes of HSA caused by echinacoside interaction were examined by evaluating the synchronous fluorescence intensity of free HSA and echinacoside-HSA complex. Based on the literature, the synchronous fluorescence spectra of HSA could provide useful information about Try and Trp residues, when the D-values ($\Delta\lambda$) between excitation and emission wavelengths were fixed at 15 and 60 nm, respectively (Gokavi et al., 2023). Fig. 5 displays the synchronous

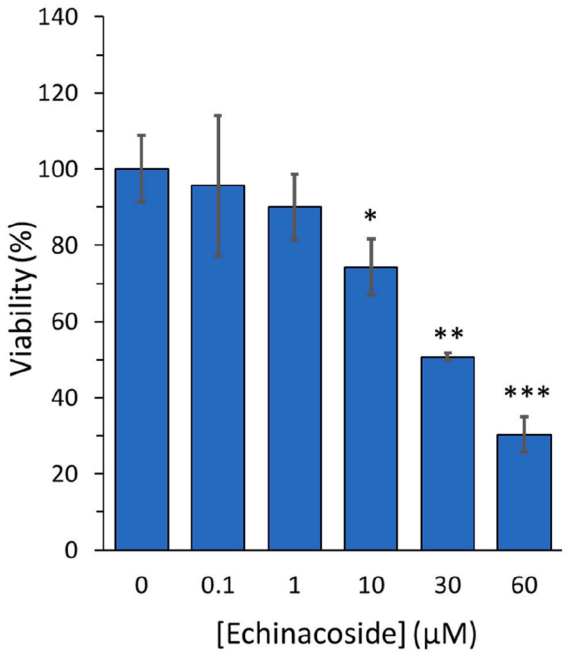

Fig. 8. MTT assay for evaluating the echinacoside's effect with various concentrations (0, 0.1, 1, 10, 30, and 60 μM) on the growth of human HCC cell line, MHCC97-H, following incubation for 24 h. *P < 0.05, **P < 0.01, ***P < 0.001 relative to control.

fluorescence spectra of HSA's Tyr (Fig. 5a) and Trp (Fig. 5b) residues following interaction with increasing concentrations of the echinacoside. An apparent blue-shift in the λ_{max} at both $\Delta\lambda = 15$ nm (Fig. 5a) and $\Delta\lambda = 60$ nm (Fig. 5b) was observed with increasing concentrations of the echinacoside.

These results demonstrated that Trp and Tyr residues positioned in a hydrophilic environment were transferred to a hydrophobic environment upon interaction of the protein with echinacoside (Esazadeh et al., 2023). Therefore, we can conclude that the interaction of the echinacoside with HSA caused slight conformational changes in the protein structure by increasing hydrophobicity around the Trp and Tyr residues (Mariam et al., 2011).

3.5. Circular dichroism (CD) study

CD, a simple and sensitive technique, is widely used to assess secondary structural changes in proteins. The far-UV CD spectrum is significantly dependent on the backbone conformational characteristics of proteins. (Meti et al., 2016). Therefore, CD spectroscopy analysis was conducted on the free HSA and HSA-echinacoside complexes. The CD spectra of HSA both alone or following interaction with increasing concentrations of the echinacoside are illustrated in Fig. 6. It can be observed that HSA shows two negative bands at 208 and 222 nm, featuring typical α-helix structure of HSA (Meti et al., 2016). The HSA's CD spectra were comparable in shape in both the free and complex form, proving that the HSA's structure is primarily α-helical even after echinacoside interaction. Also, with increasing titration of the echinacoside, the intensity of the corresponding spectra increased regularly (Fig. 6), indicating that the interaction of the echinacoside with HSA led to the conformational stability in the protein. These findings are consistent with molecular docking results, which revealed that the formation of the echinacoside-HSA complex was caused by a combination of hydrophobic and hydrophilic forces. These new forces may cause HSA to be more stable in its complex form than in its free form.

The α-helicity content of the HSA was then computed to further evaluate the effect of the echinacoside on the stability of HSA. The results revealed that the α-helicity content was around 51.81 % for free HSA which is comparable with the α-helix content reported previously (Xie et al., 2011, Wang et al., 2016). However, this amount increased to 53.39 %, 53.91 %, and 55.41 % following the addition of 5, 30 and 60 μM echinacoside, respectively. The secondary structural changes detected via the CD experiment disclosed that echinacoside stabilized HSA conformation by increasing its α-helicity.

3.6. Molecular docking study

The utilization of molecular modeling simulation can be accomplished to further analyze the probable conformation of the echinacoside–HSA complex. HSA possesses three (I, II, III) homologous domains, each of which has two subdomains A and B (He and Carter, 1992). Subdomain IIA contains Trp214, the primary amino acid residue involved in the fluorescence emission of HSA (He and Carter, 1992). Site I of HSA has a potential affinity for warfarin and site II demonstrates a great affinity for ibuprofen and some other drugs (Sudlow et al., 1976). To determine the binding site on HSA for echinacoside (Fig. 7a), molecular docking analysis was performed. Echinacoside-HSA complex with a minimum Vina score of −9.3 (kcal/mol) (Fig. 7b) was formed with the aid of non-covalent interactions derived from GLU153, PHE157, GLU188, ALA191, SER192, LYS195, LYS199, TRP214, ARG218 GLN221, ARG222, HIS288, ALA291, GLU292, VAL293, GLU294, ASN295, PRO339, TYR341, VAL343, LYS436, PRO447, CYS448, ASP451, and TYR452 amino residues [Fig. 7 c(i, ii)].

Docking analysis showed that PHE157, GLU188 and PRO447contribute to the formation of hydrophobic forces, GLU153, ASP295 and PRO399 play a key role in the formation of hydrogen bonds and LYS195 and GLU292 are involved in the formation of weak hydrogen bonds [Fig. 7 c(i, ii)].

It is noteworthy to indicate that echinacoside was surrounded by several fluorophore residues, TRP214 and TYR341 of subdomain IIA and Tyr452 of subdomain IIIA of HSA, which indicates that the interaction of the echinacoside with these aromatic amino acid residues may be responsible for fluorescence quenching and conformational changes of HSA. These data proved that hydrophobic interactions as well as hydrogen bonds could play a key role in the formation of the echinacoside–HSA complex.

3.7. Echinacoside suppresses the growth of MHCC97H cells

The MTT assay was exploited to evaluate echinacoside's cytotoxic effect on the growth of MHCC97H cells. Following a 24 h incubation period with echinacoside at various concentrations (0, 0.1, 1, 10, 30, and 60 μM), the relative vitality of MHCC97H cells was depicted in Fig. 8. After 24 h, echinacoside significantly inhibited the proliferation of MHCC97H cells at concentrations of 10, 30, and 60 μM.

It was observed that the percentage of cell viability were 100.08 % ±8.69 %, 95.62 %±18.53 %, 90.01 %±8.66 %, 74.25 %±7.38 %, 50.66 %±1.00 %, and 30.36 %±4.67 % following incubation of MHCC97H cells with 0 μM, 0.1 μM, 1 μM, 10 μM, 30 μM, and 60 μM echinacoside after 24 h. The IC_{50} concentration of the echinacoside against MHCC97H cells after 24 h was 30 μM. Dong et al. reported that echinacoside concentration-dependently mitigated the growth of human MG-63 osteosarcoma cells with an IC_{50} of 45.11 μM (Dong, Wang et al., 2022). This difference was likely derived from the variation in the detection methods as well as the type of the cells.

3.8. Echinacoside triggers the apoptosis and antimetastatic activity in MHCC97H cells

Apoptosis of MHCC97H cells treated with IC_{50} concentration of the echinacoside (30 μM) for 24 h was evaluated on a flow cytometer and the data were presented as a bar graph. Flow cytometric data indicated that apoptosis is one of the key events resulting in MHCC97-H cell death induced by echinacoside. The percentage of apoptotic cells enhanced

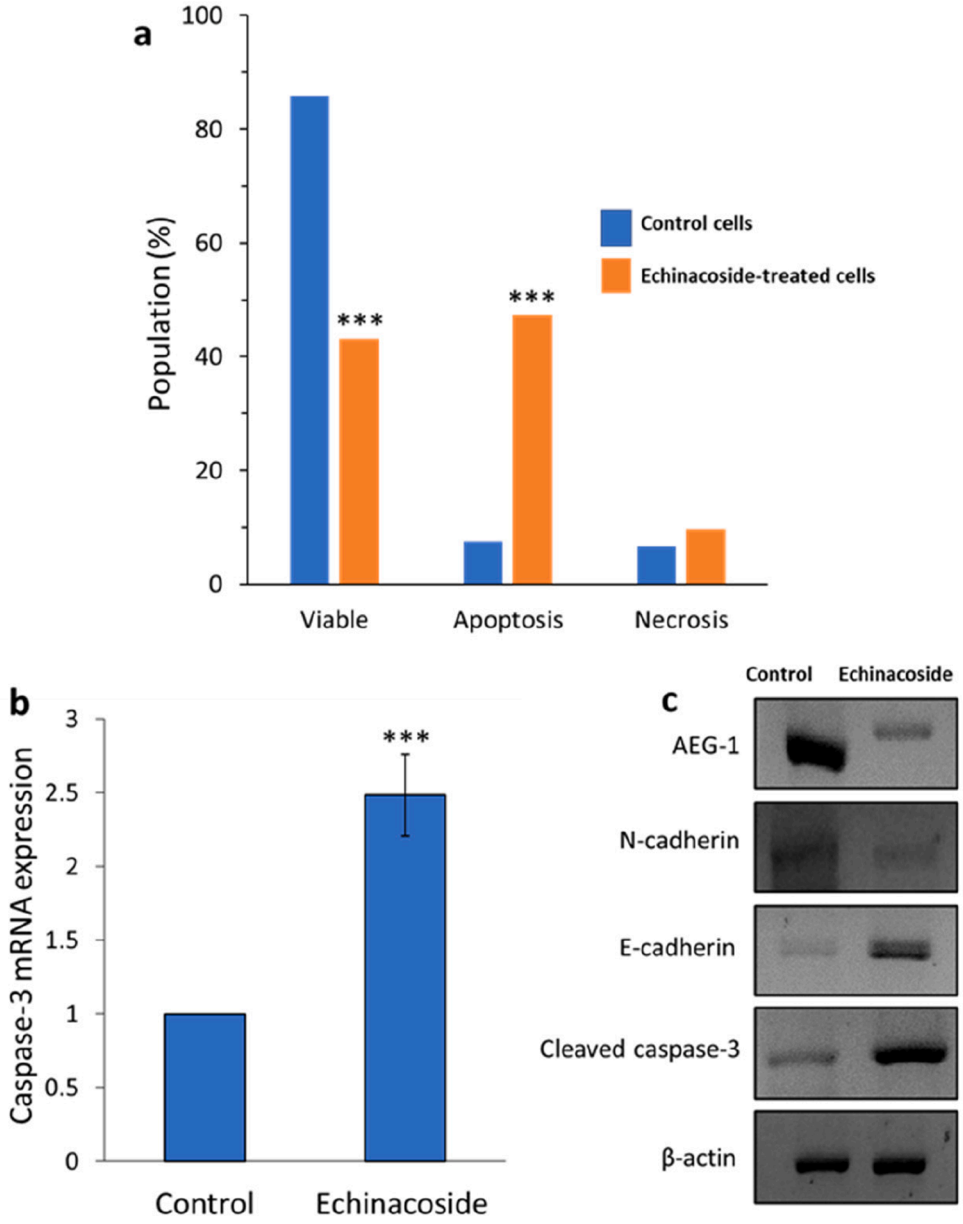

Fig. 9. Percentage of apoptosis in control MHCC97-H cell line and treated cells with IC_{50} concentration of the echinacoside (30 μM) for 24 h (a), qRT-PCR assay for evaluating the effect of IC_{50} concentration of the echinacoside (30 μM) on the caspase-3 mRNA expression of MHCC97-H cell line following 24 h incubation (b), Western blot assay for evaluating the effect of IC_{50} concentration of the echinacoside (30 μM) on the protein expression of MHCC97-H cell line following 24 h incubation (c). ***$P < 0.001$ relative to control.

with incubation of control cells (Fig. 9a) with IC_{50} concentration of MHCC97-H. The echinacoside-treated MHCC97-H cells showed a significantly higher percentage of apoptosis than the control cells (Fig. 9a). The percentage of apoptotic cells increased from 7.57 % to 47.27 % in MHCC97-H cells upon incubation with 30 μM echinacoside for 24 h (Fig. 9a).

We also used qRT-PCR and western blot assays to evaluate the effect of IC_{50} concentration of the echinacoside (30 μM) for 24 h on mRNA and protein expression of caspase-3, respectively in MHCC97-H cells. As demonstrated in Fig. 9b and c, we found that echinacoside significantly increased expressions of caspase-3 at both transcriptional and translational levels. Overexpression of caspase-3 which is known as the executor of apoptosis could be induced by the activation of caspase-8 and caspase-9 and after excessive generation of free radicals in MHCC97H cancer cells (Li, Li et al., 2014). In order to determine if the apoptosis caused by echinacoside was mediated by a caspase-dependent signaling pathway, Dong et al. used a western blot to measure the expression of caspase-3 at the protein level (Dong et al., 2015a). The results revealed treatment of SW480 colorectal cancer cells with 60 and 80 μM echinacoside for 24 h significantly elevated the level of cleaved caspase 3 (Dong et al., 2015a). Li et al., 2023 also observed similar outcomes, indicating that Huh7 and HepG2 liver cancer cells treated with various concentrations of the echinacoside displayed an elevation of caspase-3 (Li et al., 2021). Also, similar anticancer outcomes mediated by caspase-3 upregulation were shown in breast (Bian et al., 2021) and ovarian (Liu et al., 2022) cancer cells following incubation with echinacoside.

On the other hand, AEG-1 can emerge as a crucial oncogene in different processes of cancer cell development and metastasis, especially in HCC (Robertson et al., 2015, Shiragannavar et al., 2023). We then studied the impact of the echinacoside on the translational level of AEG-1 in MHCC97-H cells with western blot analysis. The results depicted

that incubation of MHCC97-H cells with IC_{50} concentration of the echinacoside (30 μM) for 24 h caused the downregulation of AEG-1 (Fig. 9c). Additionally, epithelial–mesenchymal transition (EMT) can play a key role in the progression and the metastasis of invasive HCC (Van Zijl et al., 2009, Cao et al., 2023), we, therefore, assessed whether echinacoside triggers anti-invasive and tumorigenesis in MHCC97-H cells through regulation of MET. To address this theory, we analyzed the expression of E-cadherin (epithelial markers) and N-cadherin (mesenchymal gene markers) as the main signaling hallmarks of epithelial-to-mesenchymal transition (Loh et al., 2019). As expected, incubation of MHCC97-H cells with IC_{50} concentration of the echinacoside (30 μM) for 24 h elevated the protein level of epithelial marker E-cadherin and downregulated the mesenchymal markers N-cadherin (Fig. 9c). Similar results have been reported on the inhibition of metastatic activity of MHCC97-H cells through the regulation of E-cadherin and N-cadherin triggered by Huaier polysaccharides (Zheng, Li et al., 2014).

4. Conclusion

In conclusion, as a key plasma protein that can transport various small molecules/drugs, we demonstrated that echinacoside had a potential moderate binding affinity with HSA while inducing no substantial influence on the secondary and tertiary structure of this protein. Also, we found that echinacoside can be used as an anti-metastasis drug derived from a natural source through the downexpression of AEG-1 and EMT. This data may hold great promise for *in vivo* and clinical investigations in future studies to develop potential echinacoside-mediated therapeutic derivatives that inhibit hepatocarcinogenesis and the invasion of HCC.

CRediT authorship contribution statement

Liguo Xu: Conceptualization, Methodology, Funding acquisition, Supervision, Writing – original draft. **Wenhao Huang:** Conceptualization, Methodology, Funding acquisition, Supervision. **Yachao Lin:** Investigation, Conceptualization. **Zhendong Li:** Validation, Software.

Declaration of Competing Interest

The authors declare that they have no known competing financial interests or personal relationships that could have appeared to influence the work reported in this paper.

Acknowledgments

Not applicable.

References

Bian, P., Liu, C., Hu, W., Ding, Y., Qiu, S., Li, L., 2021. Echinacoside suppresses the progression of breast cancer by downregulating the expression of miR-4306 and miR-4508. Integrative Cancer Therapies 20, 15347354–211062639.

Cao, J., Yang, S., Luo, T., Yang, R., Zhu, H., Zhao, T., Jiang, K., Xu, B., Wang, Y., Chen, F., 2023. TATA-box-binding protein promotes hepatocellular carcinoma metastasis through epithelial-mesenchymal transition. Hepatology Communications 7 (7).

Dai, Y., Han, G., Xu, S., Yuan, Y., Zhao, C., Ma, T., 2020. Echinacoside suppresses amyloidogenesis and modulates F-actin remodeling by targeting the ER stress sensor PERK in a mouse model of Alzheimer's disease. Frontiers in Cell and Developmental Biology 8, 593659.

Dennis, M.S., Zhang, M., Meng, Y.G., Kadkhodayan, M., Kirchhofer, D., Combs, D., Damico, L.A., 2002. Albumin binding as a general strategy for improving the pharmacokinetics of proteins. Journal of Biological Chemistry 277 (38), 35035–35043.

Dong, L., H. Wang, J. Niu, M. Zou, N. Wu, D. Yu, Y. Wang and Z. Zou (2015). "Echinacoside induces apoptotic cancer cell death by inhibiting the nucleotide pool sanitizing enzyme MTH1." OncoTargets and therapy: 3649-3664.

Dong, L., Yu, D., Wu, N., Wang, H., Niu, J., Wang, Y., Zou, Z., 2015b. Echinacoside induces apoptosis in human SW480 colorectal cancer cells by induction of oxidative DNA damages. International Journal of Molecular Sciences 16 (7), 14655–14668.

Esazadeh, K., Azimirad, M., Yekta, R., Dolatabadi, J.E.N., Ghanbarzadeh, B., 2023. Multi-spectroscopies and molecular simulation insights into the binding of bovine serum albumin and sodium tripolyphosphate. Journal of Photochemistry and Photobiology a: Chemistry 444, 114999.

Fan, J., Gilmartin, K., Octaviano, S., Villar, F., Remache, B., Regan, J., 2022. Using human serum albumin binding affinities as a proactive strategy to affect the pharmacodynamics and pharmacokinetics of preclinical drug candidates. ACS Pharmacology & Translational Science 5 (9), 803–810.

Flores-Rivera, M.M., Carmona-Negrón, J.A., Rheingold, A.L., Meléndez, E., 2023. 3-Ferrocenyl-estra-1, 3, 5 (10)-triene-17-one: Synthesis, Crystal Structure, Hirshfeld Surface Analysis, DFT Studies, and Its Binding to Human Serum Albumin Studied through Fluorescence Quenching and In Silico Docking Studies. Molecules 28 (16), 6147.

Gai, X., Lin, P., He, Y., Lu, D., Li, Z., Liang, Y., Ma, Y., Cairang, N., Zuo, M., Bao, Y., 2020. Echinacoside prevents hypoxic pulmonary hypertension by regulating the pulmonary artery function. Journal of Pharmacological Sciences 144 (4), 237–244.

Gao, J., Lu, W.-F., Dai, Z.-J., Lin, S., Zhao, Y., Li, S., Zhao, N.-N., Wang, X.-J., Kang, H.-F., Ma, X.-B., 2014. Induction of apoptosis by total flavonoids from Scutellaria barbata D. Don in human hepatocarcinoma MHCC97-H cells via the mitochondrial pathway. Tumor Biology 35, 2549–2559.

Geethanjali, H.S., Nagaraja, D., Melavanki, R.M., 2015. Exploring the mechanism of fluorescence quenching in two biologically active boronic acid derivatives using Stern-Volmer kinetics. Journal of Molecular Liquids 209, 669–675.

Gokavi, N.M., Nandibewoor, S.T., Gowda, J.I., 2023. Investigations of the Interaction Mechanism Between Orphenadrine Hydrochloride and Bovine Serum Albumin by Spectroscopic and Voltammetric Techniques. Journal of Fluorescence 1–13.

He, X.M., Carter, D.C., 1992. Atomic structure and chemistry of human serum albumin. Nature 358 (6383), 209–215.

He, E., Jiang, Y., Wei, D., Wang, Y., Sun, W., Jia, M., Shi, B., Cui, H., 2023. The potential effects and mechanism of the echinacoside powder in the treatment of Hirschsprung's Disease. Mathematical Biosciences and Engineering 20 (8), 14222–14240.

Holovko, O.O., Dmytrenko, O.P., Lesiuk, A.I., Kulish, M.P., Pavlenko, O.L., Naumenko, A. P., Pinchuk-Rugal, T.M., Kaniuk, M.I., Veklich, T.O., 2023. Mechanisms of the interaction of bovine serum albumin with quercetin. Molecular Crystals and Liquid Crystals 1–15.

Hu, Z.-Y., Wu, M., Wang, W.-J., Jiang, S.-L., Shi, J.-H., 2023. Exploring the binding behaviors between nisoldipine and bovine serum albumin as a model protein by the aid of multi-spectroscopic approaches and in silico. Journal of Biomolecular Structure and Dynamics 1–11.

Kaur, L., Singh, A., Datta, A., Ojha, H., 2023. Multispectroscopic studies of binding interaction of phosmet with bovine hemoglobin. Spectrochimica Acta Part a: Molecular and Biomolecular Spectroscopy 296, 122630.

Kumar, H.M.S., Kunabenchi, R.S., Biradar, J.S., Math, N.N., Kadadevarmath, J.S., Inamdar, S.R., 2006. Analysis of fluorescence quenching of new indole derivative by aniline using Stern-Volmer plots. Journal of Luminescence 116 (1–2), 35–42.

Laws, W.R., Contino, P.B., 1992. [21] Fluorescence quenching studies: Analysis of nonlinear Stern-Volmer data. Methods in Enzymology, Elsevier. 210, 448–463.

Li, P.-M., Li, Y.-L., Liu, B., Wang, W.-J., Wang, Y.-Z., Li, Z., 2014. Curcumin inhibits MHCC97H liver cancer cells by activating ROS/TLR-4/caspase signaling pathway. Asian Pacific Journal of Cancer Prevention 15 (5), 2329–2334.

Li, X., Yan, X., Yang, D., Chen, S., Yuan, H., 2023. Probing the Interaction between Isoflucypram Fungicides and Human Serum Albumin: Multiple Spectroscopic and Molecular Modeling Investigations. International Journal of Molecular Sciences 24 (15), 12521.

Li, F., Yang, Y., Zhu, P., Chen, W., Qi, D., Shi, X., Zhang, C., Yang, Z., Li, P., 2012. Echinacoside promotes bone regeneration by increasing OPG/RANKL ratio in MC3T3-E1 cells. Fitoterapia 83 (8), 1443–1450.

Li, W., Zhou, J., Zhang, Y., Zhang, J., Li, X., Yan, Q., Han, J., Hu, F., 2021. Echinacoside exerts anti-tumor activity via the miR-503-3p/TGF-β1/Smad aixs in liver cancer. Cancer Cell International 21 (1), 1–9.

Liang, Y., C. Chen, B. Xia, W. Wu, J. Tang, Q. Chen, L. Tang, H. Yang, Z. Zhang and Y. Lu (2019). "Neuroprotective effect of the echinacoside in subacute mouse model of Parkinson's disease." BioMed Research International **2019**.

Liu, J., Yang, L., Dong, Y., Zhang, B., Ma, X., 2018. Echinacoside, an inestimable natural product in treatment of neurological and other disorders. Molecules 23 (5), 1213.

Liu, J., Tang, N., Liu, N., Lei, P., Wang, F., 2022. Echinacoside inhibits the proliferation, migration, invasion and angiogenesis of ovarian cancer cells through PI3K/AKT pathway. Journal of Molecular Histology 53 (2), 493–502.

Loh, C.-Y., Chai, J.Y., Tang, T.F., Wong, W.F., Sethi, G., Shanmugam, M.K., Chong, P.P., Looi, C.Y., 2019. The E-cadherin and N-cadherin switch in epithelial-to-mesenchymal transition: signaling, therapeutic implications, and challenges. Cells 8 (10), 1118.

Mariam, J., Dongre, P.M., Kothari, D.C., 2011. Study of interaction of silver nanoparticles with bovine serum albumin using fluorescence spectroscopy. Journal of Fluorescence 21, 2193–2199.

Menezes, T.M., Seabra, G., Neves, J.L., 2023. Molecular Recognition Study toward the Mitochondrial Electron Transport Chain Inhibitor Mubritinib and Human Serum Albumin. Molecular Pharmaceutics 20 (8), 4021–4030.

Meti, M.D., Nandibewoor, S.T., Joshi, S.D., More, U.A., Chimatadar, S.A., 2016. Binding interaction and conformational changes of human serum albumin with ranitidine studied by spectroscopic and time-resolved fluorescence methods. Journal of the Iranian Chemical Society 13, 1325–1338.

Paliwal, H., Kaewpaiboon, S., M. Ali Khumaini Mudhar Bintang and T. Srichana, 2023. Interaction studies of cannabidiol with human serum albumin by surface plasmon

resonance, spectroscopy, and molecular docking. Journal of Biomolecular Structure and Dynamics 1–12.
Pilati, D., Howard, K.A., 2020. Albumin-based drug designs for pharmacokinetic modulation. Expert Opinion on Drug Metabolism & Toxicology 16 (9), 783–795.
Qiu, H., Liu, X., 2022. Echinacoside improves cognitive impairment by inhibiting Aβ deposition through the PI3K/AKT/Nrf2/PPARγ signaling pathways in APP/PS1 mice. Molecular Neurobiology 59 (8), 4987–4999.
Robertson, C.L., Srivastava, J., Rajasekaran, D., Gredler, R., Akiel, M.A., Jariwala, N., Siddiq, A., Emdad, L., Fisher, P.B., Sarkar, D., 2015. The role of AEG-1 in the development of liver cancer. Hepatic Oncology 2 (3), 303–312.
Shi, Y., H. Cao, Z. Liu, L. Xi and C. Dong (2022). "Echinacoside induces mitochondria-mediated pyroptosis through Raf/MEK/ERK signaling in non-small cell lung cancer cells." Journal of Immunology Research **2022**.
Shiragannavar, V.D., Karunakara, S.H., Puttahanumantharayappa, L.D., Sannappa Gowda, N.G., Santhekadur, P.K., 2023. Unraveling Key Signaling Pathways Altered in Hepatocellular Carcinoma. Gene Expression 22 (1), 28–40.
Sudlow, G., Birkett, D., Wade, D., 1976. Further characterization of specific drug binding sites on human serum albumin. Molecular Pharmacology 12 (6), 1052–1061.
Tang, C., Gong, L., Qiu, K., Zhang, Z., Wan, L., 2020. Echinacoside inhibits breast cancer cells by suppressing the Wnt/β-catenin signaling pathway. Biochemical and Biophysical Research Communications 526 (1), 170–175.
Tayyab, S., Sam, S.E., Kabir, M.Z., Ridzwan, N.F.W., Mohamad, S.B., 2019. Molecular interaction study of an anticancer drug, ponatinib with human serum albumin using spectroscopic and molecular docking methods. Spectrochimica Acta Part a: Molecular and Biomolecular Spectroscopy 214, 199–206.
Tyukodi, L., Zsidó, B.Z., Hetényi, C., Kőszegi, T., Huber, I., Rozmer, Z., 2023. Serum albumin binding studies on antiproliferative cyclic C5-curcuminoid derivatives using spectroscopic methods and molecular modelling. Journal of Molecular Structure 1287, 135761.
Van Zijl, F., Zulehner, G., Petz, M., Schneller, D., Kornauth, C., Hau, M., Machat, G., Grubinger, M., Huber, H., Mikulits, W., 2009. Epithelial–mesenchymal transition in hepatocellular carcinoma. Future Oncology 5 (8), 1169–1179.
Wang, W., Luo, J., Liang, Y., Li, X., 2016. Echinacoside suppresses pancreatic adenocarcinoma cell growth by inducing apoptosis via the mitogen-activated protein kinase pathway. Molecular Medicine Reports 13 (3), 2613–2618.
Wang, H., Lv, R., Gao, S., Wang, Y., Hao, N., An, Y., Li, Y., Ji, Y., Cao, M., 2023. Investigation of the interaction between the functionalized mesoporous silica nanocarriers and bovine serum albumin via multi-spectroscopy. Spectrochimica Acta Part a: Molecular and Biomolecular Spectroscopy 293, 122421.
Wang, M., Ma, X., Wang, G., Song, Y., Zhang, M., Mai, Z., Zhou, B., Ye, Y., Xia, W., 2022. Targeting UBR5 in hepatocellular carcinoma cells and precise treatment via echinacoside nanodelivery. Cellular & Molecular Biology Letters 27 (1), 92.
Xie, X., Wang, Z., Zhou, X., Wang, X., Chen, X., 2011. Study on the interaction of phthalate esters to human serum albumin by steady-state and time-resolved fluorescence and circular dichroism spectroscopy. Journal of Hazardous Materials 192 (3), 1291–1298.
Xue, P., Zhang, G., Zhang, J., Ren, L., 2021. Interaction of flavonoids with serum albumin: A Review. Current Protein and Peptide Science 22 (3), 217–227.
Yamasaki, K., Chuang, V.T.G., Maruyama, T., Otagiri, M., 2013. Albumin–drug interaction and its clinical implication. Biochimica Et Biophysica Acta (BBA)-General Subjects 1830 (12), 5435–5443.
Yammine, A., Gao, J., Kwan, A.H., 2019. Tryptophan fluorescence quenching assays for measuring protein-ligand binding affinities: principles and a practical guide. Bio-Protocol 9 (11), e3253–e.
Ye, Y., Song, Y., Zhuang, J., Wang, G., Ni, J., Xia, W., 2019. Anticancer effects of the echinacoside in hepatocellular carcinoma mouse model and HepG2 cells. Journal of Cellular Physiology 234 (2), 1880–1888.
Yekta, R., Dehghan, G., Rashtbari, S., Sheibani, N., Moosavi-Movahedi, A.A., 2017. Activation of catalase by pioglitazone: Multiple spectroscopic methods combined with molecular docking studies. Journal of Molecular Recognition 30 (12), e2648.
Yu, L., Hua, Z., Luo, X., Zhao, T., Liu, Y., 2022. "Systematic interaction of plasma albumin with the efficacy of chemotherapeutic drugs." Biochimica et Biophysica Acta (BBA)-Reviews on. Cancer 1877 (1), 188655.
Zeinabad, H.A., Kachooei, E., Saboury, A.A., Kostova, I., Attar, F., Vaezzadeh, M., Falahati, M., 2016. Thermodynamic and conformational changes of protein toward interaction with nanoparticles: a spectroscopic overview. RSC Advances 6 (107), 105903–105919.
Zhang, L., Liu, Y., Wang, Y., 2019. Interaction between an (−)-epigallocatechin-3-gallate-copper complex and bovine serum albumin: Fluorescence, circular dichroism, HPLC, and docking studies. Food Chemistry 301, 125294.
Zheng, J., Li, C., Wu, X., Liu, M., Sun, X., Yang, Y., Hao, M., Sheng, S., Sun, Y., Zhang, H., 2014a. Huaier polysaccharides suppresses hepatocarcinoma MHCC97-H cell metastasis via inactivation of EMT and AEG-1 pathway. International Journal of Biological Macromolecules 64, 106–110.
Zheng, J., Li, C., Wu, X., Yang, Y., Hao, M., Sheng, S., Sun, Y., Zhang, H., Long, J., Hu, C., 2014b. Astrocyte elevated gene-1 is a novel biomarker of epithelial–mesenchymal transition and progression of hepatocellular carcinoma in two China regions. Tumor Biology 35, 2265–2269.